

Geophysical Research Letters



RESEARCH LETTER

10.1029/2025GL117957

Key Points:

- In the future Arctic Ocean, kinetic energy increases at all depths but in particular over the top 200 m
- The mean kinetic energy associated with a spin up of the large scale circulation increases more than the eddy kinetic energy
- The increase in eddy kinetic energy is due to enhanced baroclinic instability within the mean boundary currents

Supporting Information:

Supporting Information may be found in the online version of this article.

Correspondence to:

J. K. Rieck, jan.klaus.rieck@gmail.com

Citation:

Rieck, J. K., Martínez Moreno, J., Lique, C., Dufour, C. O., & Talandier, C. (2025). Mean kinetic energy and its projected changes dominate over eddy kinetic energy in the Arctic Ocean. *Geophysical Research Letters*, 52, e2025GL117957. https://doi.org/10.1029/2025GL117957

Received 2 JUL 2025 Accepted 1 NOV 2025

Author Contributions:

Conceptualization: J. K. Rieck,

J. Martínez Moreno, C. Lique, C. O. Dufour Data curation: C. Talandier Formal analysis: J. K. Rieck, J. Martínez Moreno Funding acquisition: C. Lique, C. O. Dufour Methodology: J. K. Rieck, J. Martínez Moreno, C. Lique, C. O. Dufour

C. O. Dufour Software: J. K. Rieck, J. Martínez Moreno Visualization: J. K. Rieck

Project administration: C. Lique,

Writing – original draft: J. K. Rieck, J. Martínez Moreno

Writing – review & editing: J. K. Rieck, J. Martínez Moreno, C. Lique,

C. O. Dufour, C. Talandier

© 2025. The Author(s). This is an open access article under the terms of the Creative Commons Attribution License, which permits use, distribution and reproduction in any medium, provided the original work is properly cited.

Mean Kinetic Energy and Its Projected Changes Dominate Over Eddy Kinetic Energy in the Arctic Ocean

J. K. Rieck¹, J. Martínez Moreno^{2,3}, C. Lique², C. O. Dufour^{1,2}, and C. Talandier²

¹Department of Atmospheric and Oceanic Sciences, McGill University, Montréal, QC, Canada, ²Laboratoire d'Océanographie Physique et Spatiale (LOPS), University of Brest, CNRS, Ifremer, IRD, IUEM, Plouzané, France, ³British Antarctic Survey, Cambridge, UK

Abstract As sea ice retreats in a warming climate, the Arctic Ocean is becoming more energetic; yet little is known about this additional energy's distribution in the water column. We use a high-resolution (3–4 km) pan-Arctic ocean-sea ice model forced by present day and future scenarios to examine changes in mean kinetic energy (MKE) and eddy kinetic energy (EKE). Our study suggests that both the mean and eddy fields are becoming more energetic under anthropogenic forcing but changes in the mean circulation dominate the increase, concurrent with a spin-up of the large-scale circulation, concentrated in the top 200 m and along boundaries. The increase in EKE is strongest in the upper 50 m and is linked to enhanced baroclinic instability within the mean boundary currents. A better grasp of the distribution of this energy surplus helps to understand projected changes to stratification, mixing, and circulation in a future Arctic Ocean.

Plain Language Summary The Arctic Ocean is losing more and more sea ice due to the warming climate. As a result, more open ocean is exposed to the atmosphere. Through this open water, energy can be more efficiently transferred from the atmosphere to the ocean: the wind forces the water and creates ocean currents or changes the distribution of density, which in turn can change the currents. We show that the largest readjustment occurs for the mean circulation: the large-scale, spanning entire basins, strengthens but remains stable over time. Comparatively, less energy is transferred to small-scale, temporary ocean currents, such as eddies. This study helps to understand how changes in the transfer of energy from the atmosphere to the ocean could impact the currents, the distribution of temperature and salinity, and the layering of different water masses in a future Arctic Ocean.

1. Introduction

The ocean is experiencing significant and rapid transformations in its properties and circulation driven by anthropogenically forced changes of the climate system. In the ice-free ocean of lower latitudes, stratification has been shown to increase (Sallée et al., 2021), and the surface mesoscale ocean circulation to intensify (Beech et al., 2022; Martínez-Moreno et al., 2021). Meanwhile, in ice-covered oceans of higher latitudes, the response of oceanic circulation to climate change remains unclear due to the limited number of observations and the coarse resolution of climate models. In the Southern Ocean, a recent study by Beech et al. (2025) suggests that strong eddy activity is projected to expand into regions currently characterized by low eddy activity and to intensify along boundary currents. The Arctic Ocean is also projected to become more energetic in the future as sea ice retreats (Muilwijk et al., 2024). Yet, the details of how this increase in energy will manifest itself remain to be determined. Models of the Coupled Model Intercomparison Project Phase 6 (CMIP6) lack the resolution to capture the mesoscale variability and its projected changes, although it is thought to be crucial for lateral mixing, transport of tracers, and can feed back into the large-scale circulation (Q. Wang et al., 2024). Moreover, these models exhibit large biases in their representation of the mean circulation and stratification in the Arctic (Shu et al., 2023) that result in a large spread between projections from different models (Khosravi et al., 2022).

Recently, a kilometer-scale ocean-sea ice model forced by future atmospheric conditions simulated a large increase in eddy kinetic energy (EKE) over the top 200 m in the Arctic (Li et al., 2024). This strengthening was linked to an increase in EKE generation by baroclinic instability. However, where exactly within the top 200 m these changes occur remains to be explored. This is crucial as the current Arctic mesoscale activity exhibits a peculiar subsurface intensification driven by the presence of sea ice that both inhibits baroclinic instability and tends to dissipate surface EKE (Meneghello et al., 2021). Moreover, the relative changes affecting the partitioning

RIECK ET AL. 1 of 10

between the reservoirs of the Arctic mean kinetic energy (MKE) and EKE have yet to be determined. Globally, a recent analysis of high-resolution climate simulations suggests that the total kinetic energy may decrease in the future due to a decrease in EKE in the deep ocean, partially offset by an acceleration of large-scale circulations in the upper layer (S. Wang et al., 2024). In the Arctic, the story may be different. Over the past two decades, the total kinetic energy within the Beaufort Gyre has increased significantly. Driven by changes in atmospheric and sea ice conditions, these changes were associated with a strong spin-up of the gyre (an increase in MKE, Lin et al., 2023) but with only a small increase in EKE (Regan et al., 2020). We do not know, however, if similar trends will continue into the future.

This study investigates the impact of future anthropogenic forcing on the Arctic circulation, considering separately the mean and eddy kinetic energy, and focusing on the vertical structure within the top 350 m, where changes are strongest. We use two simulations of an Arctic Ocean model at 1/12°; one represents present-day conditions and the other is forced with the predicted forcing for 2050, thus extending previous work by creating a link between recently observed (Regan et al., 2020) and projected changes due to the loss of sea ice.

2. Model and Methods

2.1. Model

Our analysis uses two simulations performed with the high-resolution regional Arctic-North Atlantic model configuration CREG12 (Canadian Regional; Dupont et al. (2015); Regan et al. (2020)). CREG12 is based on the NEMO 3.6 (Madec & the NEMO Team, 2016) and LIM 3.5 (Rousset et al., 2015) numerical models for the ocean and sea ice components, respectively. The configuration covers the Arctic Basin and the North Atlantic down to 26° N. It has a vertical resolution of 75 levels and a horizontal resolution of 3–4 km in the Arctic Ocean. With most KE on scales >20 km (cf. Figure 4c in Li et al., 2024) and \geq 2 grid points per Rossby radius (Figure S1 in Supporting Information S1), mesoscale baroclinic eddies are resolved in the Arctic except on the shallow shelves (Dupont et al., 2015).

The first simulation ("REF") is a hindcast covering 1979–2015. Its initial conditions are from the World Ocean Atlas 2009 climatology of temperature and salinity. Initial sea ice thickness and concentration are taken from a global ORCA12 simulation performed by the Drakkar group (Tréguier et al., 2014). Along the lateral open boundaries, monthly mean conditions (3D velocities, temperature and salinity, and sea ice thickness and concentration) from the same ORCA12 simulation are applied. The Drakkar Forcing Set (DFS 5.2, which is an updated version of the forcing set described in Brodeau et al., 2010) is used as atmospheric forcing. River and ice sheet runoffs are from Hu et al. (2019) and include the large, increasing contribution from Greenland. A weak sea surface salinity (SSS) restoring nudges the surface toward the monthly climatological SSS from the World Ocean Atlas 2009 in ice-free areas to avoid excessive model salinity drift. The REF simulation is described in Talandier and Lique (2021), and an extended evaluation of the ocean and sea ice conditions in the Arctic Basin can be found in Regan et al. (2020) and Barton et al. (2022). Both the MKE and EKE in REF compare well to available observations (Figure S2 in Supporting Information S1; Armitage et al., 2017; von Appen et al., 2022a).

The second simulation ("FUT") is identical to REF, albeit its atmospheric forcing, which is representative of a future, warmer climate in 2041–2071. This atmospheric forcing is built with DFS5.2 as a baseline, to which anomalies of the filtered (31-year Hanning filter) zonal and meridional wind stress, air temperature and humidity at 2 m, shortwave and longwave radiations, snowfall and precipitation are added. These anomalies are computed as monthly anomalies (relative to 2010) of the fields from the RCP8.5 simulation performed with the GFDL-ESM2G model (Dunne et al., 2012) following the method of Receveur et al. (2021). This method allows to consider the impact of atmospheric changes on the Arctic ocean and sea ice, while limiting the impact of the well-known biases of the Arctic atmospheric conditions in coupled climate models (Bell et al., 2021; Taylor et al., 2022). Yet, we acknowledge that our framework is not fully consistent, as FUT retains open boundary conditions, runoff and SSS restoring that are representative of the historical period rather than the future. While keeping present-day boundary conditions in the North Atlantic at 26°N should not impact the Arctic much, the boundary condition in the Bering Strait represents an important source of freshwater to the Arctic and may have a greater influence on the studied region. However, CMIP6 models project a small decrease of the volume transport through Bering Strait over the 21st century (by less than 20%) and a roughly constant freshwater transport (S. Wang et al., 2022). Thus, it seems reasonable to neglect the changes in boundary conditions on the Arctic

RIECK ET AL. 2 of 10

circulation on the time scale considered. Present-day runoff and SSS restoring in FUT are assumed to lead to a less-pronounced freshening (see Section 4).

In the following, we focus on the period 1996–2015 for REF and 2051–2070 for FUT to allow for an initial spinup of the ocean and sea ice conditions. Our analysis is based on 5-day average output of the simulations.

2.2. Methods

The specific kinetic energy (KE) is computed as

$$KE = 0.5(u^2 + v^2), \tag{1}$$

where u and v are the model's 5d-mean horizontal velocities in x- and y-direction, respectively. KE is then decomposed into mean kinetic energy (MKE) and eddy kinetic energy (EKE) using a Reynolds decomposition. MKE is computed based on the sum of the horizontal velocities' annual mean and seasonal cycle's anomaly from the long-term mean, so that MKE includes the variability of the mean flow from seasonal to interannual and decadal time scales. The EKE includes variability at frequencies higher than the seasonal cycle up to 5 days, that is, all transient processes such as coherent eddies, jets, meanders, and others. This decomposition does not generally ensure that MKE + EKE = KE (Kang & Curchitser, 2017) but the residual has been found to be <2% in this study.

Surface work is calculated following Renault et al. (2016) to assess the amount of energy input to the ocean from either the atmosphere or the sea ice. The total surface work is the sum of wind work

$$FK^{a} = \frac{(1-\alpha)}{\rho_{0}} \left(\overline{\tau_{x}^{a} u} + \overline{\tau_{y}^{a} v} \right)$$
 (2)

and ice work

$$FK^{i} = \frac{\alpha}{\rho_{0}} \left(\overline{\tau_{x}^{i} u} + \overline{\tau_{y}^{i} v} \right), \tag{3}$$

where $\tau_{x,y}^a$ and $\tau_{x,y}^i$ denote the atmosphere-ocean and ice-ocean stress in x- and y-directions, respectively, α is the sea ice concentration and $\rho_0 = 1025$ kg m⁻³, a reference density. The drag coefficients c_d to calculate stresses are the same for REF and FUT with c_d^a based on Large and Yeager (2009) and $c_d^i = 0.01$.

Occurrence of baroclinic instability is estimated by the term $\overline{w'b'}$ which is proportional to the conversion from eddy potential to eddy kinetic energy (e.g., Von Storch et al., 2012), with w the vertical velocity and b the buoyancy. Buoyancy is defined as $-\frac{g}{\rho_0}(\rho-\rho_0)$, where g=9.81 m s⁻². The ' denotes a deviation from the seasonal mean as defined for MKE and the $\bar{\tau}$ denotes the 20-year average.

3. Results

3.1. Increase in Kinetic Energy Under Anthropogenic Forcing

In present-day conditions (REF), KE at the surface of the Arctic Ocean is generally reduced in regions covered with sea ice, with values ranging between 10^{-3} and 10^{-2} m² s⁻² under sea ice concentration higher than 80% compared to levels above 10^{-1} m² s⁻² in the open ocean. This is most evident along boundary currents including the Alaskan Coastal Current and in the Barents Sea (Figure 1a). While KE at 100 m depth is significantly weaker than at the surface, there is the same qualitative difference between sea ice-covered and open ocean regions, with high KE in the central Arctic concentrated along topographic features (Figure 1d). At 300 m depth, KE in the interior basin is reduced by two orders of magnitude compared to the surface. In addition to the higher KE along the boundaries, such as the Barents and Laptev Sea shelf breaks, a doubling of KE is visible along bathymetric features such as the Lomonosov Ridge and Chukchi Plateau (Figure 1g). Generally, the contrast between KE over the slopes and in the interior is enhanced at depth compared to the surface.

RIECK ET AL. 3 of 10

19448007, 2025, 22, Downloaded from https://agupubs.onlinelibrary.wiley.com/doi/10.1029/2025GL117957 by British Antarctic Survey, Wiley Online Library on [13/11/2025]. See the Terms and Conditions

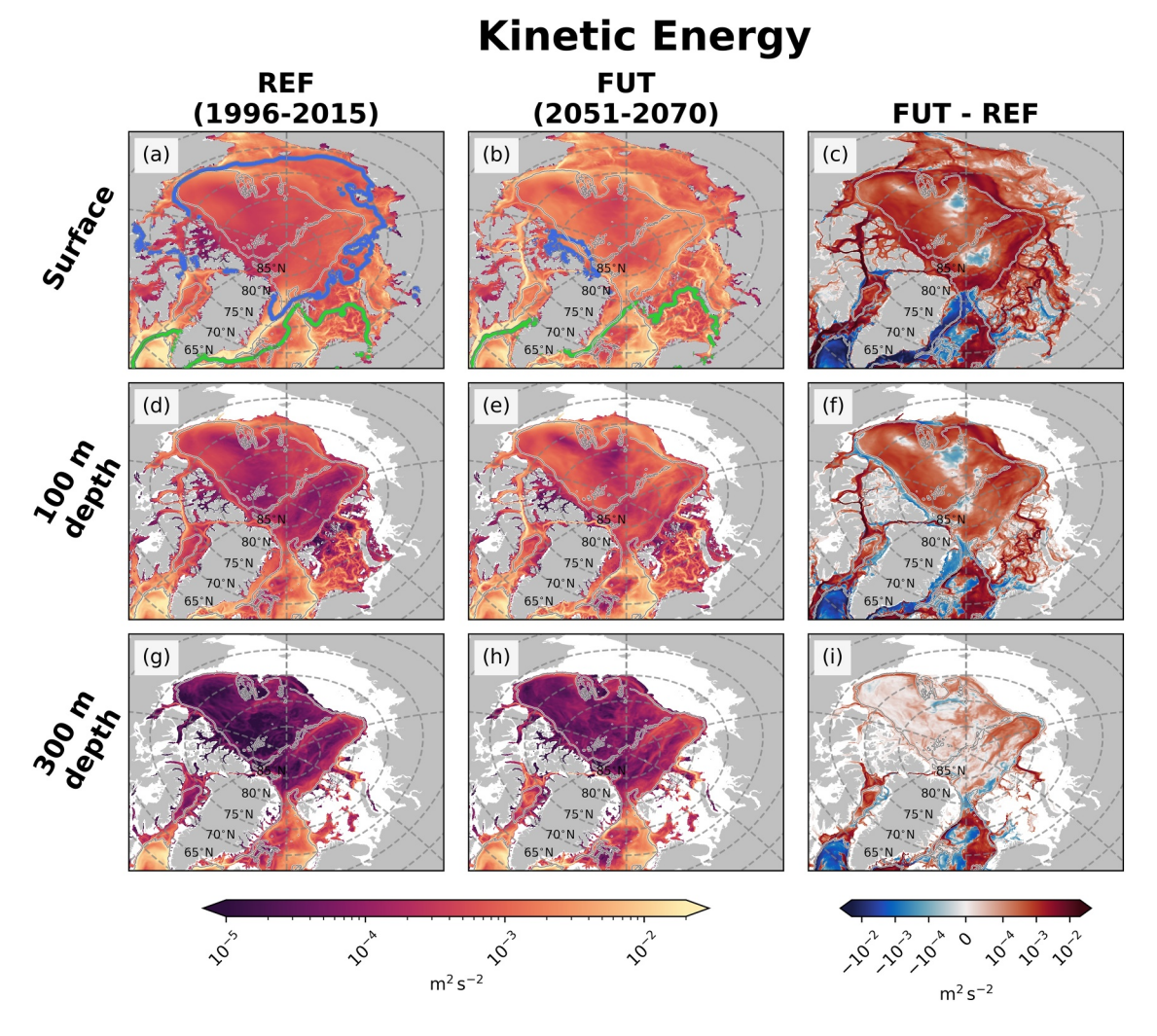


Figure 1. Kinetic Energy at the surface (a–c), 100 m depth (d–f), and 300 m depth (g–i) averaged over 1996–2015 for REF (a, d, g) and 2051–2070 for FUT (b, e, h) and the difference between FUT and REF (c, f, i). Additionally, (a, b) show average sea ice concentration of 15 and 80% as green and blue contours, respectively. The 1,500 m isobath is shown as a dashed, gray contour. Color scales are logarithmic (for REF and FUT) and symmetric logarithmic (FUT—REF).

Future conditions (FUT) show a drastic decrease in sea ice cover with only a small region north of Greenland and the Canadian Arctic Archipelago (CAA), referred to as the Last Ice Area (Pfirman et al., 2009), covered by sea ice with average concentrations higher than 80%. Accordingly, an overall KE intensification occurs at the surface (Figures 1b and 1c). In particular, the surface KE increases by an order of magnitude in FUT for regions previously covered by sea ice concentrations above 80% in REF. These changes are most intense along the Arctic boundary currents, such as the Alaskan Coastal Current and the Atlantic Water pathways along the Eurasian shelfbreak. Notably, the surface KE also increases substantially in the Last Ice Area. This increase is a first hint that the direct damping of ocean currents by sea ice is not the main driver determining the distribution of KE, consistent with the findings of Li et al. (2024). At 100 m depth, the future KE response resembles that at the surface except for a thin band along the northern limits of Greenland and the CAA where KE decreases (Figures 1e and 1f). Further down at 300 m depth, the increase in KE in FUT is concentrated along the boundaries and changes in the interior are weak (Figures 1h and 1i). Below 300 m, both KE and its future changes remain much smaller (not shown). Although this is beyond our main region of interest, we note that, at all depths, KE and its future changes are strongest in the Labrador and Greenland seas with intense weakening in the West and East Greenland currents and strengthening in the eastern Greenland Sea.

RIECK ET AL. 4 of 10

19448007, 2025, 22, Downloaded from https://agupubs

nelibrary.wiley.com/doi/10.1029/2025GL117957 by British Antarctic Survey, Wiley Online Library on [13/11/2025]. See the Terms and Conditions

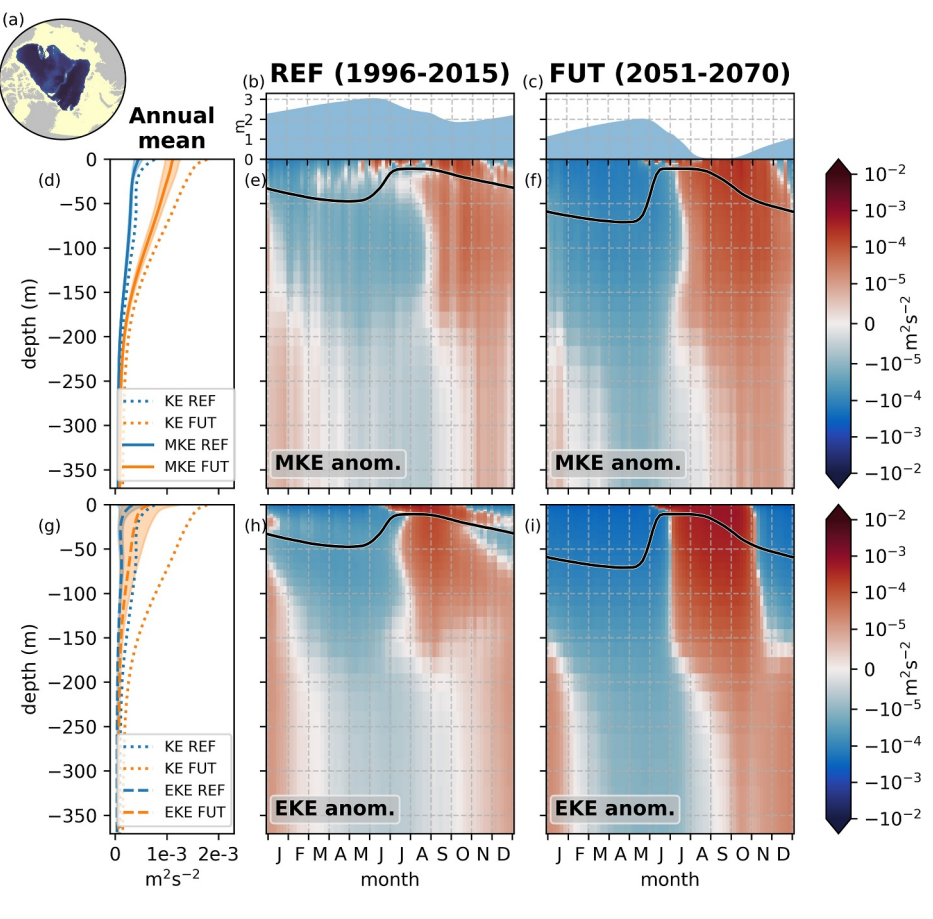


Figure 2. Climatological seasonal cycles of MKE, EKE and ice thickness averaged over the central Arctic, defined as the area of the Arctic Ocean with depth greater than 1,000 m (see the inset (a)). (b, c) Show the sea ice thickness for REF and FUT, respectively. (e, h) and (f, i) Depict the seasonal anomaly of MKE and EKE for REF and FUT, respectively. Anomalies are calculated with respect to the annual mean at each depth shown in (d, g), where blue lines indicate REF and orange lines FUT. KE is represented by dotted lines in (d, g), MKE as solid lines in (d) and EKE as dashed lines in (g). Shading around the lines in (d) and (g) depicts \pm one standard deviation. The solid black line in (e, f, h, i) shows the seasonal cycle of mixed layer depth defined as the depth where the density increase is 0.01 kg m⁻³ with respect to 10 m depth.

3.2. Vertical Structure of the Changes in Kinetic Energy

The vertical structure of the KE, MKE, and EKE seasonal cycles and their relation to the seasonal cycle of sea ice are investigated to better understand the changes of KE in the central Arctic (bathymetry >1000 m; Figure 2a). An increase of KE in the future is found at all depths but is weaker than 10^{-5} m² s⁻² below ~200 m where KE is low (Figures 2d and 2g). In REF, MKE accounts for the dominant part (70%) of KE, although the contribution of EKE is important in the upper ~20 m. Similarly, the increase of KE in concert with the reduction in sea ice in FUT is dominated by an increase in MKE (+138%; Figures 2b–2d and 2g) while the EKE's response (+117%) is mostly restricted to the surface layer (top 50 m).

Both MKE and EKE exhibit an intensified seasonality in FUT (Figures 2d, 2g, 2f, and 2i), in agreement with an enhanced seasonal cycle in sea ice thickness (Figures 2b and 2c). Indeed, in REF, the mean sea ice thickness seasonal amplitude is around 1 m, with a minimum of \sim 2 m in October and a maximum of 3 m in May/June. In contrast, the ice thickness amplitude between winter and summer increases up to 2 m in FUT, as the region is ice-free in August/September. The sea ice's impact on the seasonality of MKE and EKE in both simulations is most pronounced in the upper \sim 10 m of the water column due to the direct dynamical impact of sea ice on circulation, that is, the frictional dissipation of KE by the ice cover (Ou & Gordon, 1986) is only efficient within the Ekman layer of \sim 10 m thickness (Cole et al., 2014). In fall, when sea ice forms, the upper 10 m of the mixed layer exhibit a rapid decrease in MKE and EKE while higher levels of energy are retained into the winter deeper down (2e, f, h),

RIECK ET AL. 5 of 10

19448007, 2025, 22, Downloaded from https://agupubs.onlinelibrary.wiley.com/doi/10.1029/2025GL117957 by British Antarctic Survey, Wiley Online Library on [13/11/2025]. See

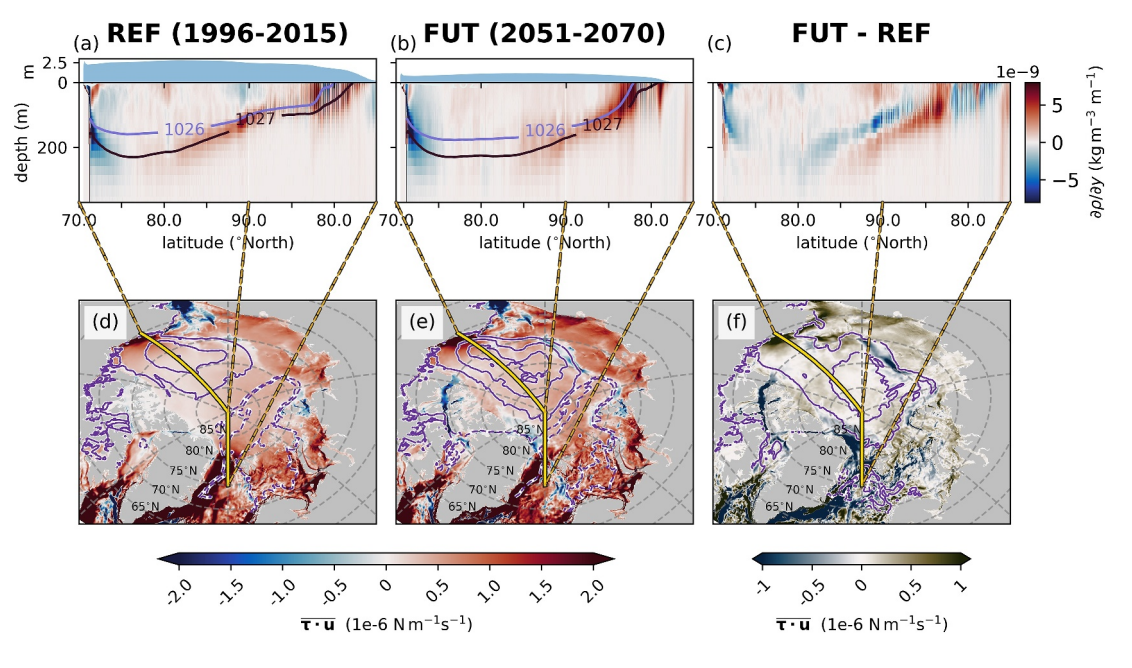


Figure 3. Mean meridional density gradients along a transect crossing the Canadian Basin, the North Pole and the western Eurasian Basin (solid golden line in (d–f)) for REF (a) and FUT (b), and the difference between FUT and REF (c). The blue and black contours in (a, b) show isopycnals of 1,026 and 1,027 kg m⁻³, respectively, of potential density referenced to the surface. Upper panels in (a, b) show the averaged ice thickness along the transects. Mean surface work in REF (d), FUT (e) and the difference between FUT and REF (f). Purple contours in (d, e) correspond to the mean barotropic streamfunction with contour intervals of 2 Sv (dashed contours indicate negative values) and the contours in (f) represent the difference between FUT and REF.

except for EKE in FUT that decreases rapidly and simultaneously from the surface down to 150 m. This decrease of EKE and the overall stronger seasonal cycles in FUT compared to REF could be related to a stronger seasonality of the sea ice that has an enhanced influence on the subsurface ocean due to a weakened stratification above 100 m depth (Figure S4 in Supporting Information S1). Below the mixed layer, two distinct layers can be discerned. (a) between the bottom of the Mixed Layer and $\sim 150-200$ m, where the seasonal cycle of both MKE and EKE remains strong and negatively correlated with the seasonal cycle in sea ice thickness, and (b) below ~ 200 m, where the seasonal cycles' amplitudes are weaker and the phases are shifted towards later in the year by 3 months. In this deeper layer, MKE increases in September for REF and July/August for FUT, while EKE tends to increase later in the year around September/October in both simulations. A possible explanation may be that EKE is following MKE, and thus an enhanced production of EKE is due to changes induced by the mean circulation. The different lag between the seasonal cycles of MKE and EKE in REF and FUT is possibly related to an increase in stratification in this layer in FUT, as stronger stratification results in a smaller growth rate of instabilities (e.g., Eady, 1949; Tulloch et al., 2011). Thus, it takes longer for the EKE to increase after an increase of MKE.

Overall, it becomes evident that MKE dominates the reservoir of KE, and its future changes are larger than changes in EKE, especially below the Ekman layer. There, the direct effect of a reduction in sea ice, that is, a loss of dissipation, cannot explain the responses of MKE and EKE to the forcing in FUT.

3.3. Driving Mechanisms of the Increase in Kinetic Energy

We further investigate possible driving mechanisms of the simulated behavior of MKE by studying changes in large-scale horizontal density gradients (Figures 3a–3c) and energy input from the atmosphere and sea ice (Figures 3d–3f). Horizontal density gradients do, in fact, increase in the future along the Alaskan slope between 70 and 75 °N and in the Eurasian Basin around 83 °N. However, the dominant signal in the interior basin is a shift of the gradients toward the Eurasian Basin over the northern flank of the Beaufort Gyre and the North Pole (Figures 3a–3c). These shifted and increased density gradients are associated with an accumulation of freshwater in the center of the Beaufort Gyre due to increased Ekman pumping (not shown) that causes a deepening of the isopycnals, especially towards the Eurasian Basin. This deepening is concurrent with a significant expansion of

RIECK ET AL. 6 of 10

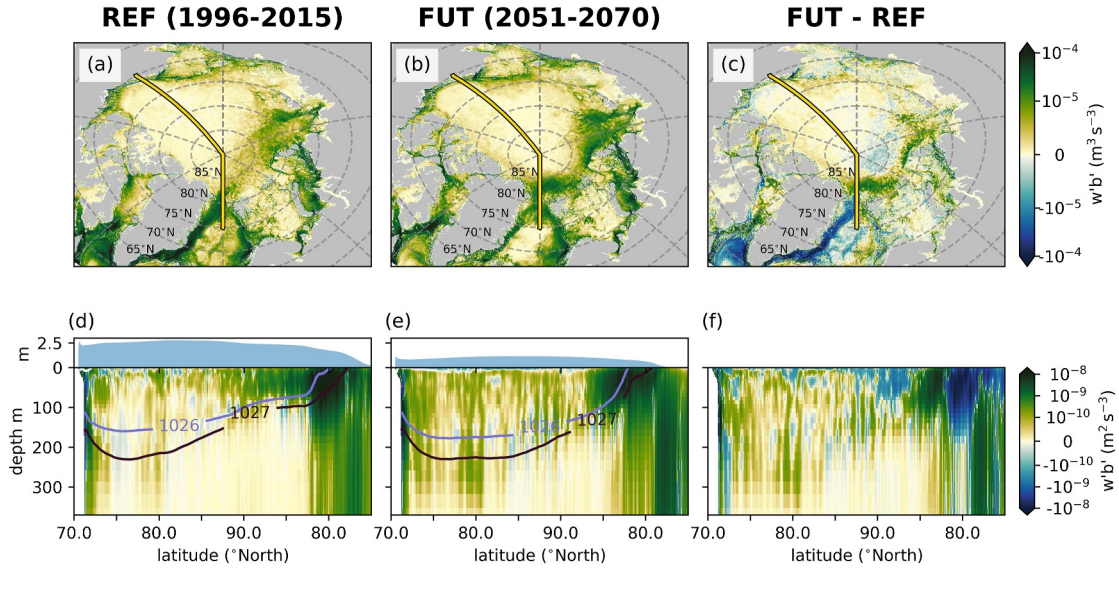


Figure 4. Mean baroclinic conversion rate (w'b'), vertically integrated over the upper 300 m in (a)–(c) and along a transect crossing the Canadian Basin, the North Pole and the western Eurasian Basin in (d)–(f) for REF in (a) and (d), FUT in (b) and (e) and the difference between FUT and REF in (c) and (f). The transect is depicted as a solid golden line in (a)–(c). Contours and upper panels in (d, e) as in Figures 3a and 3b.

the gyre as indicated by the barotropic streamfunction (Figures 3d–3f). In REF, the streamfunction has a maximum of 4 Sv in the center of the Beaufort Gyre and a cyclonic circulation in the Eurasian Basin with the zero-contour restricted to south of 85°N in the Canadian Basin. In FUT, the Beaufort Gyre intensifies and expands over a much larger area over the pole into the Eurasian Basin so that the cyclonic circulation therein is contracted. This expansion and intensification of the gyre circulation is driven by a general increase in surface work that fuels the mean circulation (Figures 3d–3f). Increased FK even occurs in regions with reduced wind speed (not shown) and is thus mostly attributable to the loss of sea ice. Some regions like the Siberian shelfbreak, the CAA and just north of Fram Strait show instead more energy loss in the future. While this loss is attributed to changes in ice-ocean work FKⁱ, the overall increase in surface work is due to increased energy input from the atmosphere FK^a in FUT (not shown). Although this larger FK^a fuels a stronger mean circulation, larger wind work also dissipates the eddy field in a process known as "eddy killing" (Renault et al., 2016) and its changes are strongest in winter (Li et al., 2024). This process could likely reduce the response of the near-surface EKE despite the decreased dissipation by sea ice in FUT.

The mean circulation's future response to the increased energy input is analogous to the interannual pattern described in Regan et al. (2020) based on the same model configuration (REF). They report a mean circulation that, although intensifying, does not become unstable due to (a) the stabilizing effect of the Alaskan shelf's slope (Manucharyan & Isachsen, 2019) and (b) the Beaufort Gyre's ability to expand toward the North, as also observed in this study. However, possibly due to the stronger forcing signal in this study, we find higher baroclinic instability in some regions, as observed in the conversion from eddy potential to eddy kinetic energy $(\overline{w'b'})$, Figure 4). The strongest increase of $\overline{w'b'}$ is observed in the Eurasian Basin in FUT, especially north of Fram Strait, with an additional increase along the Alaskan slope. This is in accordance with changes in the meridional density gradients and the barotropic streamfunction (Figure 3), as well as the potential vorticity gradients (Figure S6 in Supporting Information S1; cf. Meneghello et al., 2021). Additional regions with significantly increased $\overline{w'b'}$ are found along the Siberian Shelf and the Chukchi Borderlands. While most of the central Arctic exhibits a weaker signal in $\overline{w'b'}$ compared to the boundaries, there are significant contributions at depth below 50 m from within the Beaufort Gyre away from the shelf (Figures 4d-4f) where $\overline{w'b'}$ is low in REF. In summary, the increased MKE and EKE in FUT can be explained by a stronger energy input to the ocean leading to increased horizontal density gradients and an intensification of the Beaufort Gyre, that leads to an increase in baroclinic instability. The changes in MKE dominate over EKE, likely due to processes that prevent baroclinic instability from growing despite a more intense gyre (Regan et al., 2020).

RIECK ET AL. 7 of 10

4. Discussion and Conclusions

Utilizing a high-resolution (1/12°) ocean general circulation model forced with either present day (1996–2015) or future (2051–2070) atmospheric conditions, we examine changes in kinetic energy over the top 350 m of the Arctic Ocean (Figure 1). We find that, on average over the Arctic Basin, both MKE and EKE are increasing by 138% and 117%, respectively, yet the absolute increase of MKE is twice as large as the increase of EKE, as ~70% of KE is stored as MKE (Figures 2d and 2g). This dominance of MKE over EKE is a peculiarity of the Arctic Ocean and is likely related to the Beaufort Gyre remaining relatively stable even though more energy is transferred to the ocean from the atmosphere (Regan et al., 2020). Nevertheless, the changes to the circulation have an impact on the conversion of eddy potential energy to EKE as measured by an overall increase in $\overline{w'b'}$ (Figure 4), which is consistent with previous studies (Li et al., 2024). Importantly, the intensity of the mean circulation itself increases significantly in the future, highlighting that changes in atmospheric forcing and reduced dissipation due to the loss of sea ice have a profound impact on the mean, and not only on the eddy circulation, an aspect that has so far been overlooked in previous work.

One of the most prominent future changes of the mean circulation is a spin-up and expansion of the Beaufort Gyre into the Eurasian Basin (Figures 3d–3f). This projected expansion suggests that recently observed changes to the Beaufort Gyre's location and intensity (Lin et al., 2023; Regan et al., 2019) might represent a response to global warming and not solely be attributed to internal variability. We do not find a direct link of the Beaufort Gyre to the location and strength of the Beaufort High as in Athanase et al. (2025) as changes to the wind patterns in FUT's atmospheric forcing are not conclusive and wind stress increases even in regions of reduced wind speed (not shown). The investigation of the detailed forcing behind those changes is beyond the scope of this study, but the projected increase in surface work (Figures 3d–3f) and reduced dissipation by sea ice are likely contributors.

Both REF and FUT use the same present-day runoff and SSS restoring as future boundary conditions are unknown. Although climate models, which do not require these boundary conditions, could provide remedy, they have large biases in the Arctic (Shu et al., 2023) and insufficient resolution. As a result, the simulated response to an increased accumulation of freshwater is probably an underestimation as the mean circulation, specifically the Beaufort Gyre, is known to be impacted by increased runoff (Slater et al., 2021; Tajouri et al., 2024). Nevertheless, the mean SSS in the central Arctic decreases from 30.44 in REF to 30.29 in FUT and even though the restoring likely dampens any changes in salinity gradients across the slope, the shelfbreak and slope show a stronger intensification of MKE compared to the interior, specifically for the Alaskan Coastal Current, where the presence of the continental slope stabilizes the mean current (Regan et al., 2020).

Changes to the mean circulation do not only lead to an increased generation of EKE but also have the potential to impact the in- and outflows of the Arctic as suggested by the decreased MKE simulated along the outflow path east of Greenland and increased MKE in some channels of the Canadian Arctic Archipelago (Figure S3 in Supporting Information S1). Additionally, the changes in circulation will most certainly impact the redistribution of Atlantic Water within the Arctic and thus potentially change the hydrography, stratification and sea ice extent. At the same time buoyancy fluxes at the surface will be drastically altered due to changing sea ice conditions and atmospheric patterns, thus potentially amplifying or opposing changes due to circulation. This study shows that the impact of sea ice loss in a future Arctic Ocean goes far beyond a reduced dissipation of kinetic energy at the surface, even impacting the circulation at depth. Future studies with coupled high-resolution simulations and continued observations are needed to investigate the projected changes to an Arctic Ocean in a warming climate on a detailed, regional level to understand the possible implications.

Conflict of Interest

The authors declare no conflicts of interest relevant to this study.

Data Availability Statement

A full description of the simulations used in this study, CREG12.L75-REF08 and CREG12.L75-FUT08, as well as all the information required to produce the model outputs are available in open access from Talandier and Lique (2021, 2025), respectively. These repositories include the configuration files, the links to boundary conditions, atmospheric forcing and initialization files. All routines necessary to post-process the model output and

RIECK ET AL. 8 of 10

19448007, 2025, 22, Downloaded

create the figures shown in this manuscript along with the post-processed, final data used to create the figures are available from Rieck and Martínez Moreno (2025). Arctic geostrophic currents data that we used to compute MKE were provided by the Centre for Polar Observation and Modeling, University College London (www.cpom. ucl.ac.uk/dynamic_topography) (Armitage et al., 2017) and EKE based on observational data sets was computed from von Appen et al. (2022a, 2022b).

Acknowledgments

We thank Thomas Gorgues for providing FUT's model forcing fields. JKR and COD acknowledge support from the Natural Sciences and Engineering Research Council of Canada (NSERC) through Discovery grants (Grant RGPIN-2018-04985), Accelerator Supplements (Grant RGPAS-2018-522502), and Canada Research Chair (Grant 252794), and support of the Québec-Océan research network. We acknowledge support from the Fonds de recherche du Ouébec-Nature et technologies (FRONT) and the French Ministry of Europe and Foreign Affairs through the Samuel-de-Champlain grant (https://doi.org/10.69777/329860). CL and CT are further supported by funding from the CLIMArcTIC project funded by the "PPR Océan et Climat-France 2030" (contract ANR-22-POCE-0005). JMM and CL were funded from the ANR ImMEDIAT project (ANR-18-CE01-0010) and the MEDLEY project funded by the program JPI Ocean/JPI Climate (ANR-19-JPOC-0001). The pan-Arctic simulations were performed using HPC resources from the French GENCI-CINES center (Grants 2018-A0050107420 and 2022-A0110107420).

References

Geophysical Research Letters

- Armitage, T. W., Bacon, S., Ridout, A. L., Petty, A. A., Wolbach, S., & Tsamados, M. (2017). Arctic Ocean surface geostrophic circulation 2003–2014. *The Cryosphere*, 11(4), 1767–1780. https://doi.org/10.5194/tc-11-1767-2017
- Athanase, M., Köhler, R., Heuzé, C., Lévine, X., & Williams, R. (2025). The Arctic Beaufort Gyre in CMIP6 models: Present and future. *Journal of Geophysical Research: Oceans*, 130(4), e2024JC021873. https://doi.org/10.1029/2024JC021873
- Barton, B. I., Lique, C., Lenn, Y.-D., & Talandier, C. (2022). An ice-ocean model study of the mid-2000s regime change in the Barents Sea. Journal of Geophysical Research: Oceans, 127(11), e2021JC018280. https://doi.org/10.1029/2021JC018280
- Beech, N., Rackow, T., Semmler, T., Danilov, S., Wang, Q., & Jung, T. (2022). Long-term evolution of ocean eddy activity in a warming world. Nature Climate Change, 12(10), 910–917. https://doi.org/10.1038/s41558-022-01478-3
- Beech, N., Rackow, T., Semmler, T., & Jung, T. (2025). High-latitude Southern Ocean eddy activity projected to evolve with anthropogenic climate change. Communications Earth & Environment, 6(1), 237. https://doi.org/10.1038/s43247-025-02221-4
- Bell, J. D., Senina, I., Adams, T., Aumont, O., Calmettes, B., Clark, S., et al. (2021). Pathways to sustaining tuna-dependent Pacific Island economies during climate change. *Nature Sustainability*, 4(10), 900–910. https://doi.org/10.1038/s41893-021-00745-z
- Brodeau, L., Barnier, B., Treguier, A.-M., Penduff, T., & Gulev, S. (2010). An ERA40-based atmospheric forcing for global ocean circulation models. *Ocean Modelling*, 31(3–4), 88–104. https://doi.org/10.1016/j.ocemod.2009.10.005
- Cole, S. T., Timmermans, M.-L., Toole, J. M., Krishfield, R. A., & Thwaites, F. T. (2014). Ekman veering, internal waves, and turbulence observed under Arctic Sea Ice. *Journal of Physical Oceanography*, 44(5), 1306–1328. https://doi.org/10.1175/JPO-D-12-0191.1
- Dunne, J. P., John, J. G., Adcroft, A. J., Griffies, S. M., Hallberg, R. W., Shevliakova, E., et al. (2012). GFDL's ESM2 global coupled climate–carbon Earth system models. Part I: Physical formulation and baseline simulation characteristics. *Journal of Climate*, 25(19), 6646–6665. https://doi.org/10.1175/JCLI-D-11-00560.1
- Dupont, F., Higginson, S., Bourdallé-Badie, R., Lu, Y., Roy, F., Smith, G. C., et al. (2015). A high-resolution ocean and sea-ice modelling system for the Arctic and north Atlantic oceans. *Geoscientific Model Development*, 8(5), 1577–1594. https://doi.org/10.5194/gmd-8-1577-2015 Eady, E. T. (1949). Long waves and cyclone waves. *Tellus*, 1(3), 33–52. https://doi.org/10.1111/j.2153-3490.1949.tb01265.x
- Hu, X., Myers, P. G., & Lu, Y. (2019). Pacific water pathway in the Arctic Ocean and Beaufort Gyre in two simulations with different horizontal resolutions. *Journal of Geophysical Research: Oceans*, 124(8), 6414–6432. https://doi.org/10.1029/2019JC015111
- Kang, D., & Curchitser, E. N. (2017). On the evaluation of seasonal variability of the ocean kinetic energy. *Journal of Physical Oceanography*, 47(7), 1675–1683. https://doi.org/10.1175/JPO-D-17-0063.1
- Khosravi, N., Wang, Q., Koldunov, N., Hinrichs, C., Semmler, T., Danilov, S., & Jung, T. (2022). The Arctic Ocean in CMIP6 models: Biases and projected changes in temperature and salinity. *Earth's Future*, 10(2), e2021EF002282. https://doi.org/10.1029/2021EF002282
- Large, W. G., & Yeager, S. G. (2009). The global climatology of an interannually varying air—Sea flux data set. Climate Dynamics, 33(2–3), 341–364. https://doi.org/10.1007/s00382-008-0441-3
- Li, X., Wang, Q., Danilov, S., Koldunov, N., Liu, C., Müller, V., et al. (2024). Eddy activity in the Arctic Ocean projected to surge in a warming world. *Nature Climate Change*, 14(2), 156–162. https://doi.org/10.1038/s41558-023-01908-w
- Lin, P., Pickart, R. S., Heorton, H., Tsamados, M., Itoh, M., & Kikuchi, T. (2023). Recent state transition of the Arctic Ocean's Beaufort Gyre. Nature Geoscience, 16(6), 485–491. https://doi.org/10.1038/s41561-023-01184-5
- Madec, G., & the NEMO Team. (2016). NEMO ocean engine. Note du Pôle modélisation(27), 1–386.
- Manucharyan, G. E., & Isachsen, P. E. (2019). Critical role of continental slopes in halocline and eddy dynamics of the Ekman-Driven Beaufort Gyre. *Journal of Geophysical Research: Oceans*, 124(4), 2679–2696. https://doi.org/10.1029/2018JC014624
- Martínez-Moreno, J., Hogg, A. M., England, M. H., Constantinou, N. C., Kiss, A. E., & Morrison, A. K. (2021). Global changes in oceanic mesoscale currents over the satellite altimetry record. *Nature Climate Change*, 11(5), 397–403. https://doi.org/10.1038/s41558-021-01006-9
- Meneghello, G., Marshall, J., Lique, C., Isachsen, P. E., Doddridge, E., Campin, J.-M., et al. (2021). Genesis and decay of mesoscale baroclinic eddies in the seasonally ice-covered interior Arctic Ocean. *Journal of Physical Oceanography*, 51(1), 115–129. https://doi.org/10.1175/JPO-D-20-0054.1
- Muilwijk, M., Hattermann, T., Martin, T., & Granskog, M. A. (2024). Future sea ice weakening amplifies wind-driven trends in surface stress and Arctic Ocean spin-up. *Nature Communications*, 15(1), 6889. https://doi.org/10.1038/s41467-024-50874-0
- Ou, H. W., & Gordon, A. L. (1986). Spin-down of baroclinic eddies under sea ice. *Journal of Geophysical Research*, 91(C6), 7623–7630. https://doi.org/10.1029/JC091iC06p07623
- Pfirman, S., Tremblay, B., Fowler, C., & Newton, R. (2009). The last Arctic Sea Ice refuge. Circulation(4), 6-8.
- Receveur, A., Dutheil, C., Gorgues, T., Menkes, C., Lengaigne, M., Nicol, S., et al. (2021). Exploring the future of the Coral Sea micronekton. *Progress in Oceanography*, 195, 102593. https://doi.org/10.1016/j.pocean.2021.102593
- Regan, H. C., Lique, C., & Armitage, T. W. K. (2019). The Beaufort Gyre extent, shape, and location between 2003 and 2014 from satellite observations. *Journal of Geophysical Research: Oceans*, 124(2), 844–862. https://doi.org/10.1029/2018JC014379
- Regan, H. C., Lique, C., Talandier, C., & Meneghello, G. (2020). Response of total and eddy kinetic energy to the recent spinup of the Beaufort Gyre. *Journal of Physical Oceanography*, 50(3), 575–594. https://doi.org/10.1175/JPO-D-19-0234.1
- Renault, L., Molemaker, M. J., McWilliams, J. C., Shchepetkin, A. F., Lemarié, F., Chelton, D., et al. (2016). Modulation of wind work by oceanic current interaction with the atmosphere. *Journal of Physical Oceanography*, 46(6), 1685–1704. https://doi.org/10.1175/JPO-D-15-0232.1
- Rieck, J. K., & Martínez Moreno, J. (2025). jk-rieck/future_arctic: v1.3 (v1.3). Zenodo. https://doi.org/10.5281/zenodo.17566491

 Rousset, C., Vancoppenolle, M., Madec, G., Fichefet, T., Flavoni, S., Barthélemy, A., et al. (2015). The Louvain-La-Neuve Sea ice model LIM3.6: Global and regional capabilities. Geoscientific Model Development, 8(10), 2991–3005. https://doi.org/10.5194/gmd-8-2991-2015
- Sallée, J.-B., Pellichero, V., Akhoudas, C., Pauthenet, E., Vignes, L., Schmidtko, S., et al. (2021). Summertime increases in upper-ocean stratification and mixed-layer depth. *Nature*, 591(7851), 592–598. https://doi.org/10.1038/s41586-021-03303-x
- Shu, Q., Wang, Q., Guo, C., Song, Z., Wang, S., He, Y., & Qiao, F. (2023). Arctic Ocean simulations in the CMIP6 ocean model intercomparison project (OMIP). Geoscientific Model Development, 16(9), 2539–2563. https://doi.org/10.5194/gmd-16-2539-2023

RIECK ET AL. 9 of 10

- Slater, T., Shepherd, A., McMillan, M., Leeson, A., Gilbert, L., Muir, A., et al. (2021). Increased variability in Greenland ice sheet runoff from satellite observations. *Nature Communications*, 12(1), 6069. https://doi.org/10.1038/s41467-021-26229-4
- Tajouri, S., Llovel, W., Sevellec, F., Molines, J.-M., Mathiot, P., Penduff, T., & Leroux, S. (2024). Simulated impact of time-varying river runoff and Greenland freshwater discharge on sea level variability in the Beaufort Gyre over 2005–2018. *Journal of Geophysical Research: Oceans*, 129(9), e2024JC021237. https://doi.org/10.1029/2024JC021237
- Talandier, C., & Lique, C. (2021). ctalandi/num-exps-doi: Creg12.175-ref08 (v1.1) [Software]. Zenodo. https://doi.org/10.5281/zenodo.5789520 Talandier, C., & Lique, C. (2025). Creg12.175-fut08 (v1.0) [Software]. Zenodo. https://doi.org/10.5281/zenodo.15657723
- Taylor, P. C., Boeke, R. C., Boisvert, L. N., Feldl, N., Henry, M., Huang, Y., et al. (2022). Process drivers, inter-model spread, and the path forward: A review of amplified Arctic warming. Frontiers of Earth Science, 9, 1–29. https://doi.org/10.3389/feart.2021.758361
- Tréguier, A.-M., Deshayes, J., Le Sommer, J., Lique, C., Madec, G., Penduff, T., et al. (2014). Meridional transport of salt in the global ocean from an eddy-resolving model. *Ocean Science*, 10(2), 243–255. https://doi.org/10.5194/os-10-243-2014
- Tulloch, R., Marshall, J., Hill, C., & Smith, K. S. (2011). Scales, growth rates, and spectral fluxes of baroclinic instability in the ocean. *Journal of Physical Oceanography*, 41(6), 1057–1076. https://doi.org/10.1175/2011JPO4404.1
- von Appen, W.-J., Baumann, T., Janout, M., Koldunov, N., Lenn, Y.-D., Pickart, R., et al. (2022a). Eddies and the distribution of eddy kinetic energy in the Arctic Ocean. *Oceanography*, 35(2). https://doi.org/10.5670/oceanog.2022.122
- von Appen, W.-J., Baumann, T., Janout, M. A., Koldunov, N., Lenn, Y.-D., Pickart, R., et al. (2022b). Eddy kinetic energy in the Arctic Ocean from moored velocity observations [Dataset]. *PANGAEA*. https://doi.org/10.1594/PANGAEA.941165
- Von Storch, J. S., Eden, C., Fast, I., Haak, H., Hernández-Deckers, D., Maier-Reimer, E., et al. (2012). An estimate of the Lorenz energy cycle for the World Ocean based on the 1/10°STORM/NCEP simulation. *Journal of Physical Oceanography*, 42(12), 2185–2205. https://doi.org/10. 1175/IPO-D-12-079.1
- Wang, Q., Shu, Q., Bozec, A., Chassignet, E. P., Fogli, P. G., Fox-Kemper, B., et al. (2024). Impact of increased resolution on Arctic Ocean simulations in ocean model intercomparison project phase 2 (OMIP-2). *Geoscientific Model Development*, 17(1), 347–379. https://doi.org/10.5194/gmd-17-347-2024
- Wang, S., Jing, Z., Wu, L., Sun, S., Chen, Z., Ma, X., & Gan, B. (2024). A more quiescent deep ocean under global warming. *Nature Climate Change*, 14(9), 961–967. https://doi.org/10.1038/s41558-024-02075-2
- Wang, S., Wang, Q., Wang, M., Lohmann, G., & Qiao, F. (2022). Arctic Ocean freshwater in CMIP6 coupled models. *Earth's Future*, 10(9), 1–24. https://doi.org/10.1029/2022EF002878

RIECK ET AL. 10 of 10